

RESEARCH ARTICLE

10.1002/2015JD024173

Key Points:

- WACCM-D, including *D* region chemistry, can reproduce atmospheric effects of the January 2005 SPE
- Results show significant improvement in modeling of polar HNO_3 , HCl , ClO , OH , and NO_x
- Order-of-magnitude enhancements in HNO_3 above 45 km are in agreement with satellite data

Correspondence to:M. E. Andersson,
monika.andersson@fmi.fi**Citation:**

Andersson, M. E., P. T. Verronen, D. R. Marsh, S.-M. Päivärinta, and J. M. C. Plane (2016), WACCM-D—Improved modeling of nitric acid and active chlorine during energetic particle precipitation, *J. Geophys. Res. Atmos.*, 121, 10,328–10,341, doi:10.1002/2015JD024173.

Received 3 SEP 2015

Accepted 12 AUG 2016

Accepted article online 16 AUG 2016

Published online 1 SEP 2016

WACCM-D—Improved modeling of nitric acid and active chlorine during energetic particle precipitation

M. E. Andersson¹, P. T. Verronen¹, D. R. Marsh², S.-M. Päivärinta^{1,3}, and J. M. C. Plane⁴¹Earth Observation, Finnish Meteorological Institute, Helsinki, Finland, ²Atmospheric Chemistry Division, National Center for Atmospheric Research, Boulder, Colorado, USA, ³Department of Physics, University of Helsinki, Helsinki, Finland,⁴School of Chemistry, University of Leeds, Leeds, UK

Abstract Observations have shown that a number of neutral minor species are affected by energetic particle precipitation (EPP) and ion chemistry (IC) in the polar regions. However, to date the complexity of the ion chemistry below the mesopause (i.e., in the *D* region ionosphere) has restricted global models to simplified EEP/IC parameterizations which are unable to reproduce some important effects, e.g., the increase of mesospheric nitric acid (HNO_3). Here we use WACCM-D, a variant of the Whole Atmosphere Community Climate Model which includes a selected set of *D* region ion chemistry designed to produce the observed effects of EPP/IC. We evaluate the performance of EPP/IC modeling by comparing WACCM-D results for the January 2005 solar proton event (SPE) to those from the standard WACCM and Aura/Microwave Limb Sounder (MLS) and SCISAT/Atmospheric Chemistry Experiment-Fourier Transform Spectrometer (ACE-FTS) observations. The results indicate that WACCM-D improves the modeling of HNO_3 , HCl , ClO , OH , and NO_x during the SPE. Northern Hemispheric HNO_3 from WACCM-D shows an increase by 2 orders of magnitude at 40–70 km compared to WACCM, reaching 2.6 ppbv, in agreement with the observations. For HCl and ClO , the improvement is most pronounced in the Southern Hemisphere at 40–50 km where WACCM-D predicts a decrease of HCl and increase of ClO by 1.6% and 10%, respectively, similar to MLS data. Compared to WACCM, WACCM-D produces 25–50% less OH and 30–130% more NO_x at 70–85 km which leads to better agreement with the observations. Although not addressed here, longer-term NO_x impact of ion chemistry could be important for polar stratospheric ozone and middle atmospheric dynamics.

1. Introduction

Energetic particle precipitation (EPP) affects the mesosphere and lower thermosphere (MLT) in the polar regions and significantly influences neutral composition and dynamics of the atmosphere [Rozanov *et al.*, 2005; Seppälä *et al.*, 2009; Funke *et al.*, 2011; Rozanov *et al.*, 2012]. For example, ionization caused by solar electrons and protons leads to the production of odd hydrogen ($\text{HO}_x = \text{H} + \text{OH} + \text{HO}_2$) and odd nitrogen ($\text{NO}_x = \text{N} + \text{NO} + \text{NO}_2$) species that have significant implications for the ozone (O_3) chemistry [Jackman *et al.*, 2001; Verronen *et al.*, 2006; Jackman *et al.*, 2008]. By absorbing a great part of UV radiation, ozone plays an important role in the energy budget and dynamics of the middle atmosphere. It has been shown that the ozone changes in the stratosphere, in general, contribute to the ground-level climate variability, particularly at high latitudes [Gillet and Thompson, 2003]. Ozone variability caused by EPP in the upper stratosphere and mesosphere has been proposed to have a similar effect, although more research is needed to establish the coupling all the way to the surface [Seppälä *et al.*, 2009; Baumgaertner *et al.*, 2011; Andersson *et al.*, 2014].

Understanding all observed atmospheric effects of EPP requires a good representation of ion chemistry in models [Funke *et al.*, 2011]. Due to its complexity, the lower ionosphere (*D* region) ion chemistry is typically parameterized in global atmospheric models, and only production of HO_x and NO_x is considered. However, both satellite observations and ion chemistry analysis have shown that EPP and ion chemistry affect also other important species, such as nitric acid (HNO_3), hydrogen chloride (HCl), and chlorine monoxide (ClO) [Winkler *et al.*, 2009; Verronen *et al.*, 2011; Damiani *et al.*, 2012; Verronen and Lehmann, 2013]. These effects should not be neglected because it has been proposed that they, e.g., ionic production of HNO_3 , can lead to modulation of middle atmospheric dynamics in the polar regions [Kvissel *et al.*, 2012]. Although detailed 1-D ion chemistry models exist, global models including vertical and horizontal transport can improve our understanding of

ion chemistry impacts because they allow for long-term (e.g., solar cycle) studies and their results are more comparable to satellite observations.

The solar proton event (SPE) of 16–21 January 2005 was characterized by two solar eruptions which perturbed the middle atmosphere on both short (days) and long (weeks) time scales [Damiani *et al.*, 2008; Jackman *et al.*, 2011]. Satellite observations, as well as model simulations, showed significant enhancements in HO_x and NO_x in the polar mesosphere and, consequently, substantial ozone destruction [Seppälä *et al.*, 2006; Verronen *et al.*, 2006; Damiani *et al.*, 2008; Seppälä *et al.*, 2008]. Moreover, precipitation of solar high-energy protons elevated the amount of HNO_3 in the stratosphere/lower mesosphere and caused changes in chlorine species [Verronen *et al.*, 2011; Damiani *et al.*, 2012].

In this paper, we utilize a variant of the Whole Atmosphere Community Climate Model (WACCM) which includes a selected set of lower ionospheric (D region, <90 km) ion chemistry (WACCM-D, see Verronen *et al.* [2016] for a description). We will demonstrate how the ion chemistry in WACCM-D improves the modeling of several important middle atmospheric neutral species during the January 2005 solar proton event. This is done by comparing WACCM-D results to satellite observations as well as to the results from the standard WACCM.

2. Modeling

WACCM is a chemistry-climate general circulation model with vertical domain extending from the surface to 5.9×10^{-6} hPa (~ 140 km geometric height). The standard horizontal resolution used is 1.9° latitude by 2.5° longitude. The representation of WACCM physics in the MLT and simulations of the atmospheric response to solar and geomagnetic forcing variations are described by Marsh *et al.* [2007]. Details of recent centennial scale coupled simulations using the current version of WACCM (version 4) and an overview of the model climate can be found in the study by Marsh *et al.* [2013]. The chemistry module in WACCM is interactive with the dynamics through transport, radiative transfer, and exothermic heating. Photochemistry associated with ion species (O^+ , NO^+ , O_2^+ , N_2^+ , and N^+) is part of the standard chemistry package. The standard model uses a lookup table parameterization for HO_x production, based on the work of Solomon *et al.* [1981]. For NO_x , it is assumed that 1.25 N atoms are produced per ion pair with branching ratios of 0.55/0.7 for $\text{N}^4\text{S}/\text{N}^2\text{D}$, respectively [Jackman *et al.*, 2005; Porter *et al.*, 1976]. This parameterization is strictly valid only in the heterosphere, because its fundamental assumption is a fixed N_2/O_2 ratio, and it has been shown to underestimate NO_x production above about 65 km [Nieder *et al.*, 2014].

WACCM-D is a variant of WACCM in which the standard parameterization of HO_x and NO_x production is replaced by a set of D region ion chemistry reactions, with the aim to reproduce better the observed effects of EPP on the mesosphere and upper stratosphere neutral composition. The ion chemistry set was selected based on the current knowledge of ion chemical reactions and their effects on the neutral atmosphere [Verronen and Lehmann, 2013], and it includes 307 reactions of 20 positive ions and 21 negative ions. More details about WACCM-D as well as its lower ionospheric evaluation are presented in the companion paper by Verronen *et al.* [2016].

In this study, we have used WACCM version 4 simulations with the preconfigured specified dynamics scenario (SD-WACCM), which is forced with meteorological fields (temperature, horizontal winds, and surface pressure) from NASA GMAO (GEOS5.1) [Reinecker *et al.*, 2008] at every dynamics time step below about 50 km; above this, the model is fully interactive (88 levels in total). Note, however, that the model dynamics at all altitudes (also above 50 km) are very much driven by the winds and wave fluxes applied below 50 km, such that the internal variability of SD-WACCM is small. For example, the root-mean-square of temperature differences between the runs with and without D region chemistry indicates that there is an agreement within 3 K (i.e., 2%) in the polar regions at 60–80 km. The runs include forcing from auroral electrons and solar protons but do not include higher energy electrons (>10 keV) or galactic cosmic rays. Two model runs were made: (1) a reference run (SD-WACCM) and (2) a run with D -region ion chemistry (SD-WACCM-D). Both runs covered the period 1 January–28 February 2005. In the modeling, we use the SPE ionization rates based on GOES-11 observations and described in Jackman *et al.* [2011]. Note, however, that we excluded the highest energy protons (300–20,000 MeV) affecting altitudes below 10 hPa.

In order to have the model results comparable to the satellite observations, WACCM profiles were output at Aura Microwave Limb Sounder (MLS) and SCISAT Atmospheric Chemistry Experiment-Fourier Transform

Table 1. MLS and ACE-FTS Data Characteristics

Data	Vertical Range (hPa/km)	Vertical resolution (km)	Precision	Accuracy (%)
MLS OH	1–0.003/49–84	2.5–5	0.5–3.3×10 ⁶ cm ⁻³	10
MLS O ₃	1–0.02/49–76	3–5.5	0.2–1.4 ppbv	5–35
MLS HNO ₃	10–0.01/32–80	3–5	0.7–1.2 ppbv	10–50
MLS ClO	22–1/26–50	3–4.5	0.1–0.3 ppbv	5–20
MLS HCl	22–1/26–50	3–4	0.2–0.5 ppbv	10
ACE NO _x	4–0.005/40–85	3–4	0.6–250 ppbv	10–35

Spectrometer (ACE–FTS) observation times and locations. From these, daily averages were calculated for polar latitudes. In the case of HNO₃, the Aura/MLS averaging kernels have been applied to the model output, which decreases the HNO₃ mixing ratios at 65–75 km and increases them at 45–55 km (e.g., by a factor of 1.5–4 and 1.25–1.75, respectively, as shown by Verronen *et al.* [2011, Figure 2]). For the other species, the model results (daily averages) were simply interpolated to the same vertical grid with the observations before making a direct comparison or calculating differences between the model results and observations.

3. Satellite Observations

The Microwave Limb Sounder (MLS, <http://mls.jpl.nasa.gov>) is an instrument on board the Aura satellite [Waters *et al.*, 2006]. Aura is in a near-polar 705 km altitude orbit. As Earth rotates underneath it, the Aura orbit stays fixed relative to the Sun and gives daily global coverage with about 15 orbits per day. The local solar time is nearly the same for each orbit on a given day and at latitudes 60–90°N varies between about 1 A.M. and 1 P.M. The equatorial crossing time of the Aura satellite is about 1:30 in the afternoon. We use Version 3.3 Level 2 daily mean OH, O₃, and HNO₃ data for the period 1–31 January 2005, concentrating on latitudes 60–82.5° in the Northern Hemisphere (NH). Additionally, we use HCl and ClO observations at latitudinal band 60–82.5° in the Northern Hemisphere (NH) and in the Southern Hemisphere (SH). Before the analysis, the data were screened according to the MLS data description and quality document [Livesey *et al.*, 2011]. More information on these MLS data products is given in Table 1 and in Pickett *et al.* [2008], Jiang *et al.* [2007], Santee *et al.* [2007, 2008], and Froidevaux *et al.* [2008]. Note that we use HNO₃ observations outside the recommended altitude range, i.e., between about 40 and 80 km (2.15–0.01 hPa) [Santee *et al.*, 2007; Livesey *et al.*, 2011]. At these altitudes, the signal-to-noise ratio of the measurements is typically low because the HNO₃ mixing ratios are low. However, the HNO₃ enhancement during the SPE improves the signal-to-noise ratio and allows us to study the changes in the upper stratosphere/lower mesosphere. The HNO₃ observations contain real atmospheric signal up to about 70 km (0.046 hPa), as discussed in Verronen *et al.* [2011].

The Atmospheric Chemistry Experiment-Fourier Transform Spectrometer (ACE-FTS, <https://databace.scisat.ca/level2/>) is an instrument on board the SCISAT satellite [Bernath *et al.*, 2005]. The principle of ACE measurement is the solar occultation technique. A high inclination (74°), low Earth orbit (650 km) gives coverage of tropical, midlatitudes, and polar regions. The instrument observes the wavelengths between 2.2 and 13.3 μm during sunset and sunrise and measures vertical profiles (10–150 km) of temperature, pressure, density, and 18 atmospheric constituents, including NO and NO₂. We use NO_x observations (version 3) for the period 1 January–28 February 2005. The ACE observations were taken in the latitude range from about 57 to 66°N. More information on ACE-FTS NO_x is given in Table 1 and in Kerzenmacher *et al.* [2008]. We use NO_x observations (version 3) for the period 1 January–28 February 2005. Measurement errors for NO_x vary with altitude and time. Between 25 and 45 km, the errors are quite small (less than 20%) but increase above 45 km (less than 35%).

4. Results and Discussion

Significant perturbations were observed in short-lived species, such as OH and ozone, as a consequence of the January 2005 SPE. Figure 1 shows the MLS OH measurements (Figure 1a) together with WACCM (Figure 1b) and WACCM-D (Figure 1c) model predictions for 14–24 January 2005 in the latitude band 60–82.5°N. Both MLS and the models show large OH enhancement during the SPE. The observed and modeled increase of OH occurred on 17–18 January at altitudes between 60 and 82 km. In general, WACCM and WACCM-D agree well with observations. However, it is clear from Figure 1 that WACCM predictions overestimate OH values by about

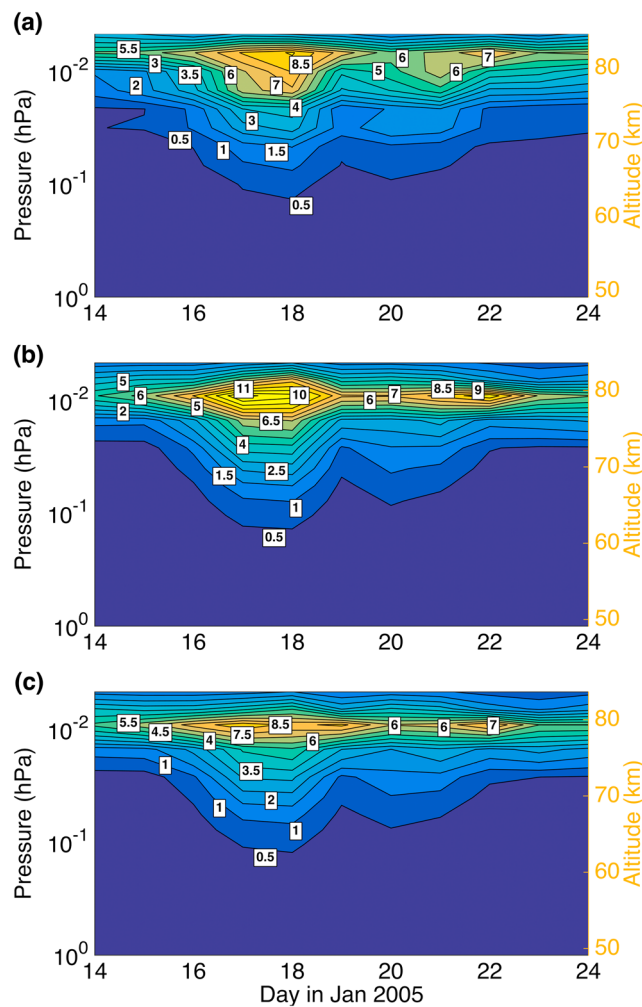


Figure 1. Daily averaged OH mixing ratio (ppbv) from (a) Aura MLS measurements and model predictions from (b) WACCM and (c) WACCM-D for the 60–82.5°N band for the period 14–24 January 2005. The contour intervals are: 0.25, 0.5, 0.75, 1, 2, 4, 6, 8, 9, 10, and 11 ppbv. MLS data uncertainty ($2 \times \text{SEM}$) varies between 0.05 and 0.25 ppbv (2–8%).

1–2.5 ppbv (20–50%) at altitudes between 60 and 80 km. The relative differences between the simulated and observed OH presented in Figure 2 indicate that during the main peak of the SPE (17 January), WACCM overestimates the OH enhancement by up to about 55% at altitudes between 60 and 80 km. The agreement between WACCM-D and observations is much better with a maximum 22% OH overestimate for the same altitudinal range. Between 60 and 80 km, WACCM-D fits better inside the MLS standard error of the mean (SEM) than WACCM which is outside SEM for almost all altitudes. Due to the short lifetime of OH [Pickett *et al.*, 2006], the changes caused by the SPE lasted only for couple of days. After 21 January, the OH observed/predicted enhanced values returned to the levels before the event.

Similar behavior in OH can be seen in Figure 3, where we compare the MLS polar maps of OH at 70–80 km with the model predictions. For clarity, measurements and predictions are shown in the latitude range 40–82.5°N, gridded into 5° latitude \times 30° longitude bins. Before the SPE on 16 January, the observed and predicted OH values are low, however, both model versions seem to overestimate the OH values. On 17 January (peak of SPE), a substantial increase of OH inside the polar cap area (poleward 60°) is observed by MLS and predicted by WACCM and WACCM-D. However, WACCM-D is in better agreement with the observations compared to WACCM, which overestimates the OH amounts over the entire polar cap, in average by about 15–35%. As discussed by Verronen and Lehmann [2013], the standard parameterization of HO_x production used in WACCM (and many other models) is dependent upon altitude and ionization rate only and neglects the effects of negative ion chemistry (e.g., HNO_3 production) and seasonal variation caused by different atmospheric conditions. At the altitudes shown in Figure 3, there is less direct HO_x production in WACCM-D, mostly because the ion

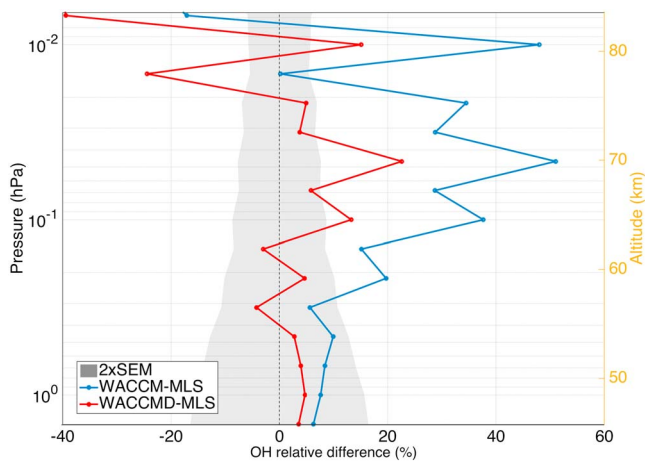


Figure 2. OH relative differences (%) between WACCM and MLS (blue line) and WACCM-D and MLS (red line) in the NH polar region on 17 January 2005. Grey area indicates MLS data uncertainty ($2 \times \text{SEM}$).

chemistry is affected by the modeled wintertime amount of water vapor, while the standard parameterization assumes a fixed summertime amount (the latter being higher). The ionic HO_x production is especially sensitive to water vapor at 70–80 km because H_2O , decreasing with increasing altitude, gradually becomes the limiting factor for water cluster ion formation. A much smaller proportion of the OH difference comes from OH/H partitioning which in WACCM parameterization is 50/50 but depends somewhat on ionization rate and altitude in WACCM-D.

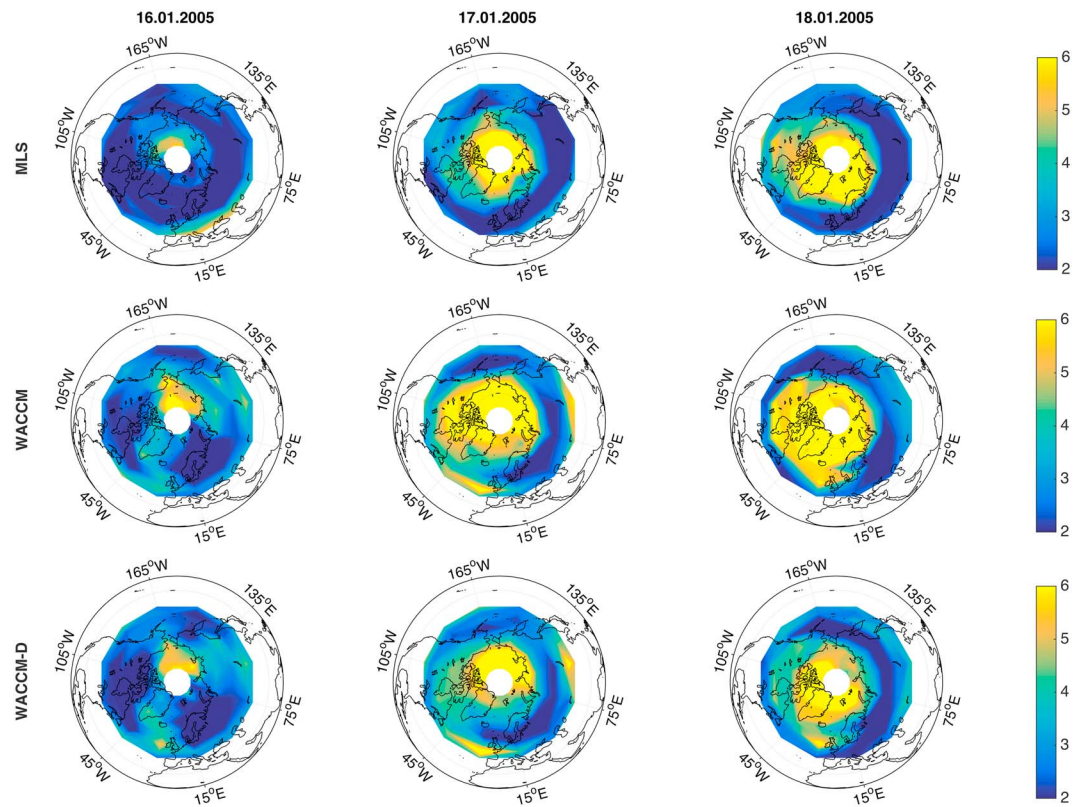


Figure 3. Polar maps of daily averaged OH mixing ratio (ppbv) from (top row) Aura MLS measurements and model predictions from (middle row) WACCM and (bottom row) WACCM-D averaged between 70 and 78 km altitude for three selected days: 16–18 of January 2005. For clarity, measurements are shown in the latitude range 40–82.5°N. MLS data uncertainty ($2 \times \text{SEM}$) varies between 0.5 and 1.5 ppbv.

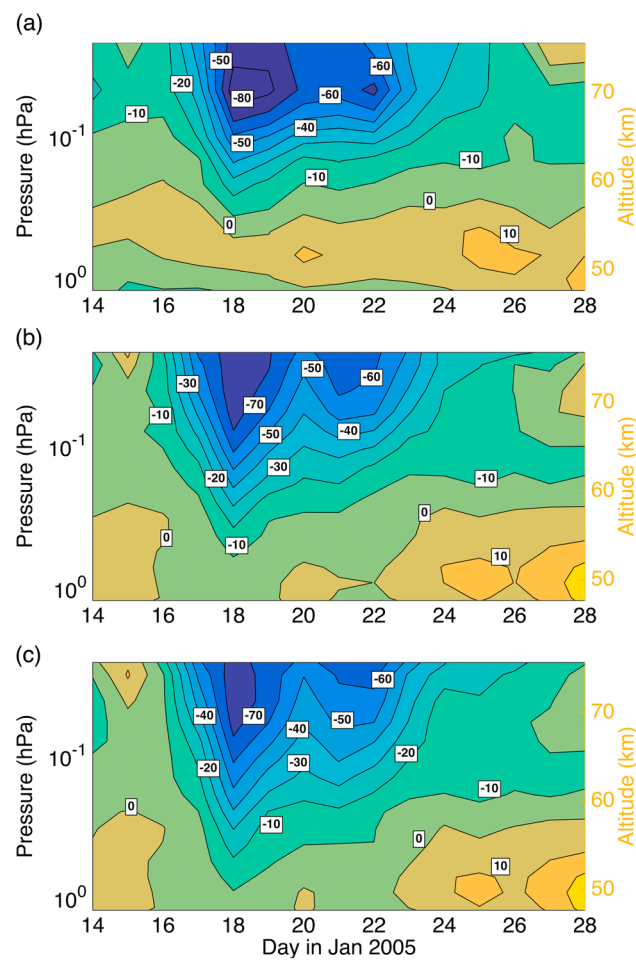


Figure 4. Daily averaged O_3 changes (%) from (a) Aura MLS measurements and model predictions from (b) WACCM and (c) WACCM-D for the $60\text{--}82.5^\circ\text{N}$ band. An observed/predicted O_3 profile for the period 1–14 January 2005 was subtracted from the observed/predicted O_3 values for the plotted days (14–28 January 2005). The contour intervals for the ozone changes are -80 , -60 , -50 , -40 , -30 , -20 , -10 , 0 , 10 , and 20% . MLS data uncertainty ($2\times\text{SEM}$) varies between 0.02 and 0.06 ppmv (5–20%).

An important consequence of the SPE-induced short-term OH enhancement is ozone loss in the upper stratosphere and mesosphere, as shown in Figure 4. The observed and modeled O_3 anomalies (%) are calculated on a daily time scale with respect to the 1–14 January average (a quiet, non-SPE period). During the SPE, ozone decreases of up to about 80% are observed by MLS and up to about 70% predicted by both WACCM and WACCM-D. Both models are in reasonably good agreement with the observations considering the magnitude of the ozone changes. At altitudes between 70 and 75 km, the observed relative ozone changes are slightly larger than predicted by WACCM and WACCM-D; however, the differences are within data uncertainty which is about 10–20%. The predicted ozone loss extends deeper than in the observations, down to about 50–55 km, as already noted earlier by Jackman *et al.* [2011, Figure 7]. The ozone depletion lasts for about 6 days (16–21 January), after which there is a gradual recovery to the levels seen before the event. The timing of ozone loss and recovery is well captured by both models. It has been shown before that the short-term mesospheric ozone depletion during SPEs can be reasonably well modeled using a simple parameterization of HO_x production [e.g., Funke *et al.*, 2011]. Our results, i.e., the relatively small differences between the WACCM and WACCM-D ozone responses, confirm this and also indicate that the water cluster ion chemistry in WACCM-D is working as expected and causing an effect which is in agreement with observations.

To summarize the short-term SPE effects, Figure 5 shows the observed and predicted OH (Figure 5a) and O_3 (Figure 5b) mixing ratios averaged between 70 and 76 km altitude and latitudes between 60 and 82.5°N . The increased OH values between 16 and 21 January coincide closely with decreased O_3 as seen from satellite

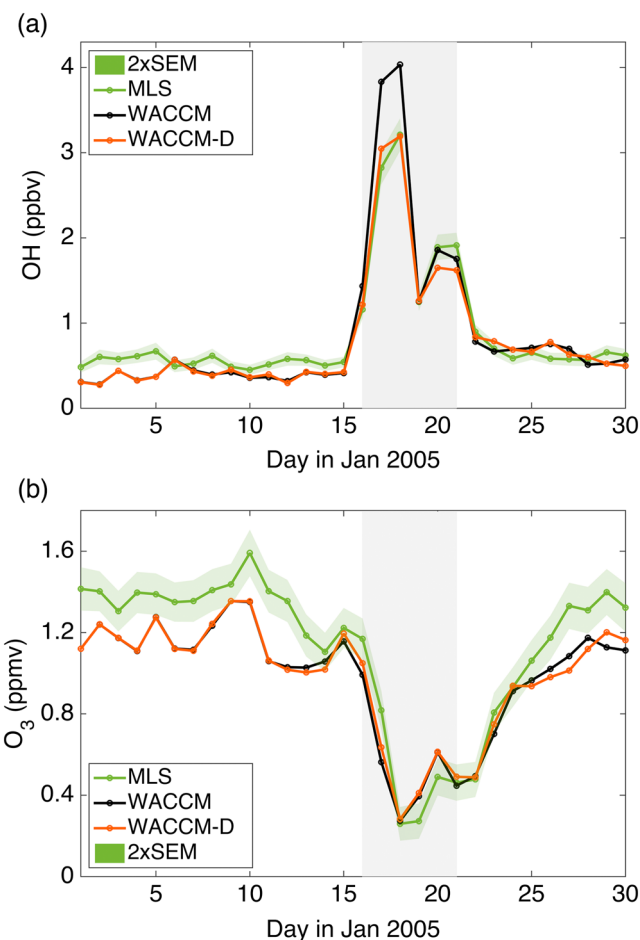


Figure 5. Daily averaged (a) OH mixing ratio (ppbv) and (b) O₃ mixing ratio (ppmv) from Aura MLS measurements together with model predictions from WACCM and WACCM-D for the 60–82.5°N band and altitudes between 70 and 76 km. SPE days are marked as a grey area. Green area indicates MLS data uncertainty ($2 \times$ SEM).

measurement and model predictions. The predicted OH enhancement by WACCM is about 35% higher than OH predicted by WACCM-D and measured by MLS. As already mentioned, the OH differences between the models are related to differences in direct HO_x production and HO_x partitioning. In the case of ozone, both WACCM and WACCM-D agree very well with observations (within data uncertainty) during and a few days after the SPE, while at other times the models predict smaller amounts of ozone.

In addition to the short-term effects, the SPE has an impact on constituents that have longer lifetimes (such as NO_x, HNO₃) and can significantly affect the atmosphere for several weeks following the event. In the absence of solar radiation, e.g., during polar winters, NO_x is chemically long-lived throughout the middle atmosphere and can be transported down from the mesosphere-lower thermosphere to the stratosphere. Once in the stratosphere, it is always long-lived and can cause catalytic ozone loss in solar illuminated conditions. During the whole of January, large amounts of NO_x were observed (Figure 6a) with a rather moderate response during and after the SPE between 16 and 31 January. In comparison, the simulated NO_x (Figures 6b and 6c) exhibits a distinctive peak corresponding to the SPE event. Moreover, during the whole period under consideration (1 January–28 February 2005), the NO_x values predicted by WACCM (Figure 8b) and WACCM-D (Figure 8c) are considerably smaller than the ACE-FTS measurements. These results confirm previous studies by Jackman et al. [2011] where ACE-FTS data and WACCM version 3 were used. One possible reason for model underestimation is the omission of medium energy electrons, because energetic electron precipitation (EEP) could produce a considerable amount of NO_x in situ in the mesosphere [e.g., Newnham et al., 2011]. In the present case, the beginning of the year was characterized by strong geomagnetic activity and EEP events that occurred during 2–7 January. Work is ongoing to include this source of EEP and it will be the topic of a future study.

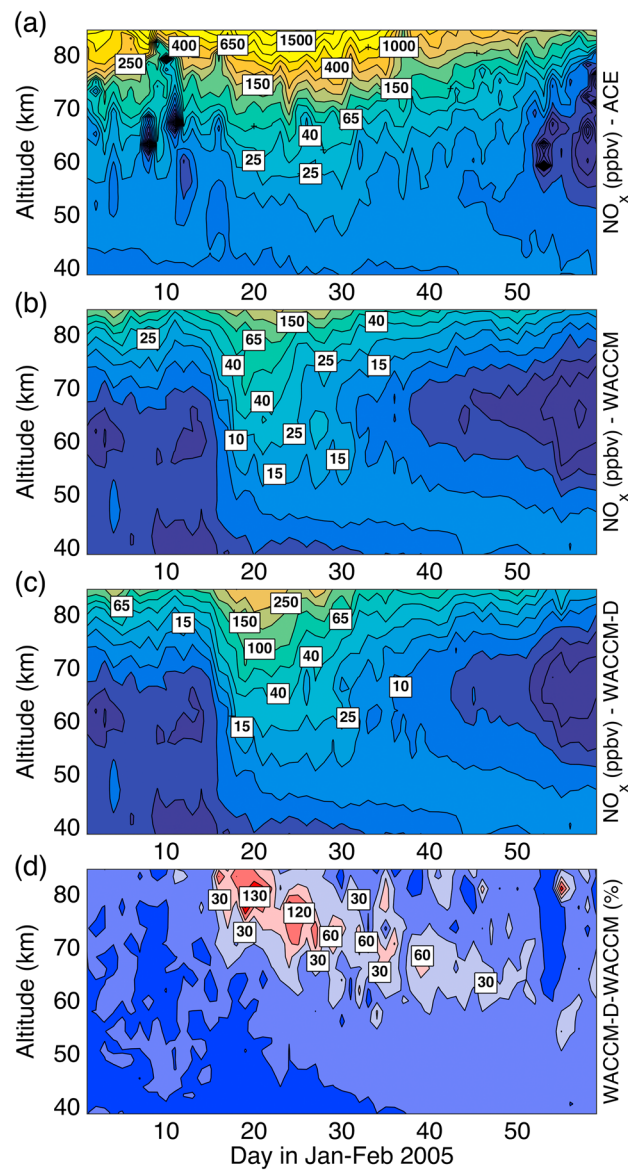


Figure 6. Daily averaged NO_x mixing ratio ($\log_{10}(\text{ppbv})$) from (a) ACE measurements and model predictions from (b) WACCM and (c) WACCM-D in the NH polar region for the first 60 days in 2005. The contour intervals are: 0.8, 1.2, 1.6, 2, 2.4, 2.8, and 3.2 \log_{10} (ppbv). Daily averaged NO_x relative differences (%) between (d) WACCM-D and WACCM in the NH polar region for the first 60 days in 2005. The contour intervals are: 0, 30, 60, 90, and 120%.

Compared to WACCM, at 60–85 km WACCM-D predicts more NO_x between days 16 and 50 (Figure 6d), caused by larger NO_x production during the SPE. As shown by Nieder *et al.* [2014], the standard parameterization used in WACCM (and many other models) underestimates NO_x production at altitudes above 65 km. This is confirmed by the differences in NO_x production between WACCM and WACCM-D: compared to the altitude-independent production of 1.25 N atoms per ion pair in WACCM, in WACCM-D the production increase with altitude reaching 2 and 2.5 N atoms per ion pair at 80 km and 100 km, respectively (not shown). These numbers are also about 50% higher than those presented by Nieder *et al.* [2014], mostly due to enhanced production from $\text{O}_2^+ + \text{N}_2 \rightarrow \text{NO}^+ + \text{NO}$ which subsequently leads to more production from $\text{NO}^+ + \text{e}^- \rightarrow 0.2\text{N}^4\text{S} + 0.8\text{N}^2\text{D} + \text{O}$ as well. Note that the former reaction produces NO directly, instead of N, and was not considered in their model by Nieder *et al.* [2014]. The difference in NO_x production is not caused by the temperature difference (which is small, only about 3 K or 2% between the models, not shown), and not

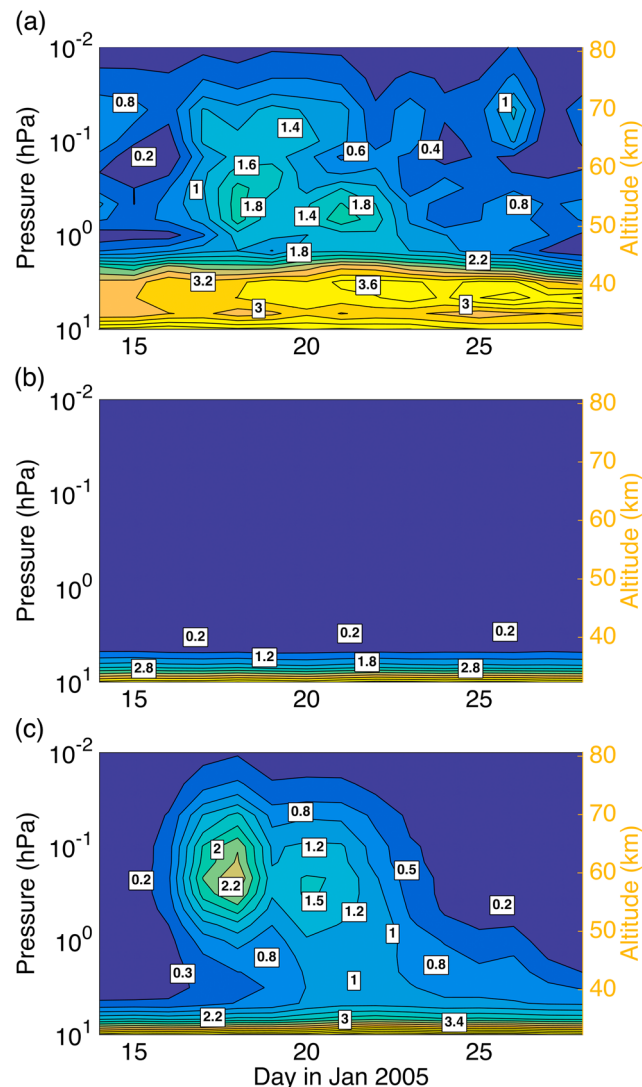


Figure 7. Daily averaged HNO_3 mixing ratio (ppbv) from (a) Aura MLS measurements and model predictions from (b) WACCM and (c) WACCM-D for the 60–82.5°N band and for the period 14–28 January 2005. The contour intervals are: 0.2, 0.4, 0.6, 1, 1.4, 1.8, 2.6, and 3.6 ppbv. MLS data uncertainty ($2 \times \text{SEM}$) varies between 0.01 and 0.15 ppbv (10–20%).

likely by the difference in atomic oxygen (up to 35% difference, not shown) because the NO_x production is not sensitive to O below about 85 km [Nieder et al., 2014]. The large differences below 70 km, after the SPE, are caused by NO_x descent from above.

Atmospheric models using an EPP lookup table parametrization, such as WACCM, significantly underestimate HNO_3 values during SPEs when compared to observations [Jackman et al., 2008; Funke et al., 2011]. In WACCM-D, HNO_3 is directly produced by ion-ion recombination reactions (as described in Verronen and Lehmann [2013]). As an example of the WACCM-D evaluation, Figure 7 shows daily averaged MLS HNO_3 (Figure 7a) together with the WACCM and WACCM-D predictions (Figures 7b and 7c, respectively) for the latitudes 60–82.5°N. During the SPE, significant enhancement of MLS HNO_3 was observed at altitudes between about 40 and 75 km. Elevated HNO_3 values (0.6–1.8 ppbv) lasted for about 10 days (16–24 of January) with the maximum increases on 17 and 21 January, when the proton fluxes were high. For comparison, the HNO_3 values predicted by WACCM are almost 100 times lower (0.03–0.04 ppbv) than those seen from satellite observations. In contrast, WACCM-D and its ion chemistry are able to reproduce the observed changes in HNO_3 . The SPE effects predicted by WACCM-D, i.e., the magnitude of the observed HNO_3 changes (0.6–2.5 ppbv), duration of the enhancement (~ 10 days) as well as affected altitudes (40–75 km), are all in good agreement with observations (within data uncertainty). Note that because the mesospheric production of HNO_3 is

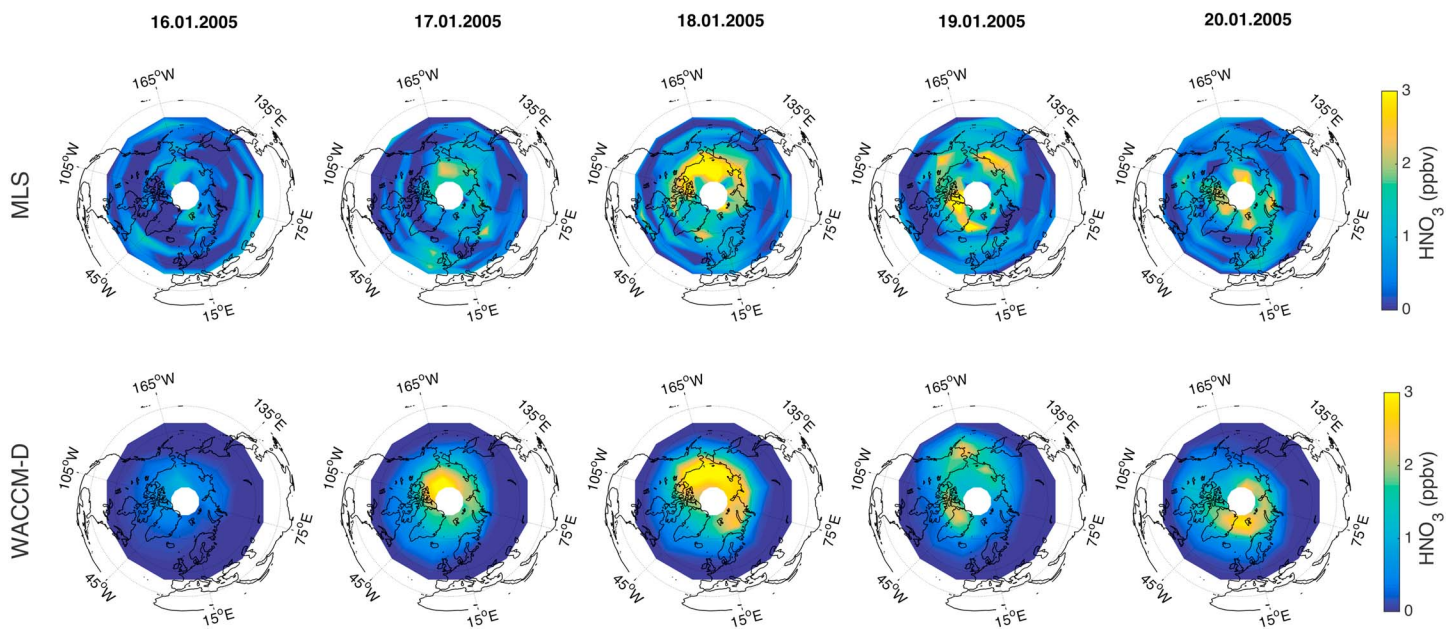


Figure 8. Polar maps of daily averaged HNO_3 mixing ratio (ppbv) from (top row) Aura MLS measurements and model predictions from (bottom row) WACCM-D averaged between 45 and 80 km altitude during the SPE between 16 and 20 January 2005. For clarity, measurements are shown in the latitude range 40–82.5°N. MLS data uncertainty ($2 \times \text{SEM}$) varies between 0.5 and 1 ppbv.

dominated by ion chemistry during large EPP events, measurements of HNO_3 changes are also a direct indicator of the EPP ion pair production rates such that they can be used as a proxy for the EPP fluxes. In the present case, the reasonably good agreement between WACCM-D and MLS gives confidence in the SPE fluxes used in the model.

This agreement between WACCM-D and the satellite observations of HNO_3 can be seen throughout the whole SPE in Figure 8. It illustrates a comparison between the observed and predicted polar maps of mixing ratios averaged between 45 and 80 km for the period 16–20 January. Around the SPE peak (17–18 of January), WACCM-D HNO_3 values are overestimated, but the differences with MLS are small. Overall, the HNO_3 distribution over the polar cap and the magnitude of the HNO_3 changes during the SPE are similar in the WACCM-D results and the observations. As already noted by Verronen *et al.* [2011], the observed HNO_3 enhancements show inhomogeneous longitudinal distribution, with a clear day-to-day variation due to atmospheric dynamics. Figure 8 shows that WACCM-D is reproducing this longitudinal variability reasonably well. Note that for reasons of clarity, the WACCM results are not shown in the figure, as the HNO_3 changes are negligible.

In general, the differences between observed and predicted HNO_3 vary with altitude and ionization levels. To demonstrate this dependency, daily averaged HNO_3 profiles from MLS measurements and model predictions from WACCM and WACCM-D for the 60–82.5°N are shown in Figure 9 (top row). It is clear that the best agreement between WACCM-D and the MLS measurements coincides with the highest ionization levels (around 17–19 January) and two altitude ranges: 45–85 and 15–35 km. In the absence of strong proton ionization, the differences are larger (e.g., on 15 and 24 January). This can also be seen in Figure 9 (bottom row), which shows the daily mean HNO_3 averaged between 45 and 80 km in January 2005. WACCM-D reproduces the enhancement in HNO_3 around the SPE period quite well (15–27 January), and the differences are within the standard error of the mean. During the quiet time conditions (no SPE ionization), the HNO_3 levels are too low compared to the MLS observations. Again, this is likely due to the omission of medium energy electron ionization in the WACCM-D model. Part of the observed HNO_3 variation at the beginning of January could be connected to the EEP event that occurred between 2 and 7 January. In comparison to WACCM-D, WACCM is unable to reproduce any changes seen in HNO_3 and the values are substantially underestimated during the whole period under consideration. Note that at around 35–45 km both models underestimate the

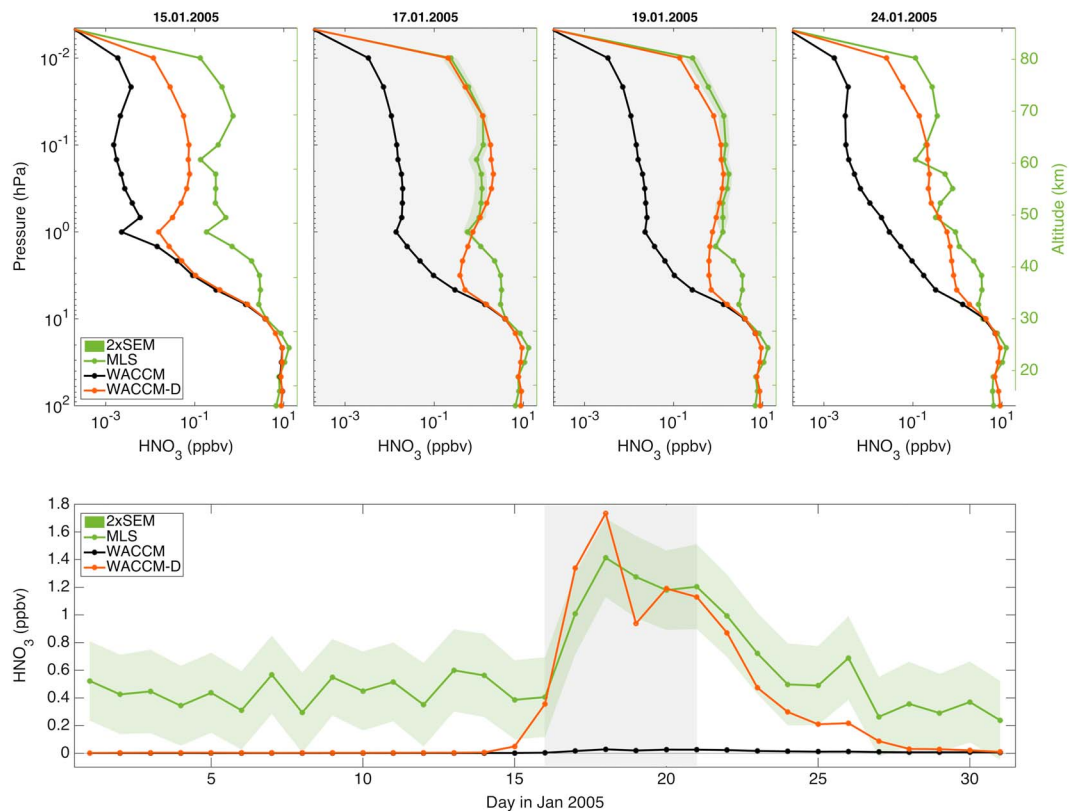


Figure 9. (top row) Daily averaged HNO₃ profiles (ppbv) from Aura MLS measurements and model predictions from WACCM and WACCM-D for the 60–82.5°N band for four selected days: 15 of January (before SPE event), 17 and 19 of January (during SPE event), and 24 of January (after SPE event). (bottom row) Daily averaged HNO₃ mixing ratio (ppbv) from Aura MLS measurements together with model predictions from WACCM and WACCM-D for the 60–82.5°N band and altitudes between 45 and 80 km. SPE days are marked as a grey area. Green area indicates MLS data uncertainty ($2 \times$ SEM).

measured HNO₃. This is explained by previous studies, which have shown that WACCM fails to reproduce the polar HNO₃ enhancements reaching the stratopause due to a low bias in the climatological distribution of N₂O₅ in the upper stratosphere [Kvissel *et al.*, 2012].

Finally, we test the capabilities of WACCM-D to reproduce the changes in chlorine species, particularly hydrogen chloride (HCl) and chlorine monoxide (ClO) which play an important role in the Cl_y family. HCl is an important reservoir of active chlorine and has been shown to respond to SPEs, partly because chlorine ion chemistry converts it to Cl, ClO, and HClO [Winkler *et al.*, 2009]. Previously, the impact of the January 2005 SPE on the chlorine family has been studied in detail by Damiani *et al.* [2012] using satellite measurements and model simulations. They found that mixing ratios of both HCl and ClO decreased in the NH during the event. Comparing WACCM-D with WACCM and the MLS observations, Figure 10 shows daily averaged anomalies of HCl and ClO for the latitudinal band 60–82.5° in the NH and SH, at altitudes between 40 and 52 km. During the SPE, satellite observations and model results show a rapid HCl decrease of about 2–6% in both hemispheres due to uptake into negative ions (Cl[−], Cl[−](H₂O), ClO[−], and NO₃[−](HCl)), starting from 16 of January. WACCM-D agrees better with the MLS HCl measurements and is able to reproduce the loss of about 4% and 1.6% in the NH and SH, respectively, during the SPE. WACCM underestimates the HCl decrease compared to MLS, especially in the SH where no response to the SPE is seen. The improvement from WACCM to WACCM-D is due to the ion chemistry converting HCl to other chlorine species. This is seen also in ClO, with WACCM-D producing a clear increase of about 10% in the SH and less decrease in the NH compared to WACCM, which leads to better agreement with the MLS observations. In the NH, the decrease of HCl and increase of ClO due to ion chemistry are only part of the change in these species (the part indicated by the difference between WACCM-D and WACCM), with a decrease of ClO beginning already a few days before the SPE in the MLS observations.

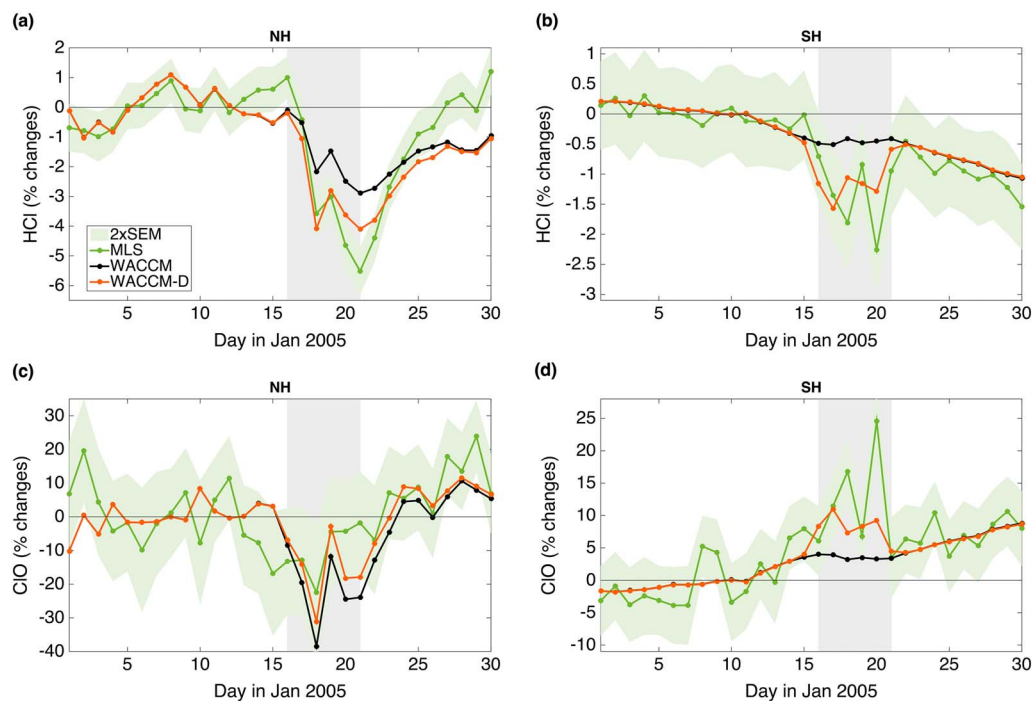


Figure 10. Daily averaged (a, b) HCl and (c, d) ClO anomalies (%) from Aura MLS measurements and model predictions from WACCM and WACCM-D for the 60–82.5°N (Figures 10a and 10c) and 60–82.5°S (Figures 10b and 10d) band and altitudes between about 40 and 50 km. An observed/predicted HCl/ClO profile for the period 1–14 January 2005 was subtracted from the observed/predicted HCl/ClO values for the plotted days (1–30 January 2005). SPE days are marked as a grey area. Green area indicates standard error of the mean (SEM). Green area indicates MLS data uncertainty ($2 \times \text{SEM}$).

5. Summary

WACCM-D is a variant of the Whole Atmosphere Community Climate Model, including a selected set of *D* region ion chemistry. Here we have evaluated WACCM-D capabilities by examining its ability to reproduce the atmospheric effects of the January 2005 solar proton event. We have validated the WACCM-D results against Aura/MLS and SCISAT/ACE-FTS satellite observations and compared the WACCM-D results to those from standard WACCM (including no *D* region ion chemistry). The results indicate that including an ion chemistry scheme in the atmospheric models can improve the EPP response of important neutral species.

The most pronounced improvement is in the modeling of HNO_3 , which is produced during SPEs mostly by ion-ion recombination reactions. Northern Hemispheric HNO_3 values above 45 km from WACCM-D are almost 100 times higher (0.6–2.6 ppmv) than those from WACCM (0.03–0.04 ppbv). Compared to MLS observations, WACCM-D was able to reproduce not only the magnitude of the observed HNO_3 changes but also the altitude distribution of the SPE-driven enhancement. The generally good agreement between WACCM-D and satellite observations (within MLS data uncertainty at most altitudes between 45 and 80 km) can be seen throughout the SPE period. Outside the SPE period and below 45 km, there is still an underestimation of HNO_3 in WACCM-D.

Ion chemistry affects also the chlorine species. Compared to MLS observations, WACCM-D ion chemistry improves the modeling of HCl and ClO. The improvement is most pronounced in the SH at 40–50 km where WACCM-D predicts a decrease of HCl and an increase of ClO by 1.6% and 10%, respectively, in general agreement with MLS observations. WACCM, without *D* region ion chemistry, does not predict any SPE-related changes in the SH.

WACCM-D simulated OH enhancement was compared to the MLS OH observations and found to be in better agreement than predictions from WACCM. During the SPE, mean OH values at altitudes 70–76 km are within the data uncertainty. Both WACCM and WACCM-D predictions show quantitatively similar O_3 depletion, which agree well with the observed MLS O_3 .

In the case of NO_x , the WACCM and WACCM-D simulations generally reproduce well the production below 70 km during the SPE. At 70–85 km, WACCM-D produces up to 130% more compared to WACCM which leads to better agreement with ACE-FTS observations. However, at these altitudes the NO_x values from both WACCM and WACCM-D are substantially smaller than ACE measurements. Underestimation of NO_x in WACCM and WACCM-D can be partially connected to the fact that the electron precipitation event in early January is not considered in the model experiments.

Although the short-term ozone response does not change much, we must emphasize that there is evidence of longer-term impact of ion chemistry on NO_x and ozone [Kvissel et al., 2012] which cannot be modeled with the ion chemistry parametrization used in WACCM. During polar winter, NO_x produced by EPP in the MLT region descends to lower altitudes [e.g., Seppälä et al., 2007; Randall et al., 2009; Salmi et al., 2011; Funke et al., 2014]. Observations have shown that, gradually over the winter, the descending NO_x can be converted first to N_2O_5 and then to HNO_3 by cluster ion reactions, which can lead to modulation of stratospheric ozone and polar vortex dynamics in model simulations [Kvissel et al., 2012, and references therein]. Since ozone is the most likely connector between EPP, atmospheric dynamics, and climate variability, it is thus important to describe ion chemistry adequately in models. Although in this paper we only consider the short-term effects of EPP, to validate the WACCM-D ion chemistry, the longer-term impacts of ion chemistry will be the topic of a future study.

Acknowledgments

The work of M.E.A., P.T.V., and S-M.P. was supported by the Academy of Finland through the projects #276926 (SECTIC: Sun-Earth Connection Through Ion Chemistry), #258165, and #265005 (CLASP: Climate and Solar Particle Forcing). D.R.M. was supported in part by NASA grant NNX12AD04G. The National Center for Atmospheric Research is operated by the University Corporation for Atmospheric Research under sponsorship of the National Science Foundation. J.M.C.P. is supported by the UK Natural Environment Research Council (grant number NE/J02077X/1). D.R.M. and P.T.V. would like to thank the International Space Science Institute, Bern, Switzerland for supporting the "Quantifying Hemispheric Differences in Particle Forcing Effects on Stratospheric Ozone" team. All model data used are available from corresponding author by request (monika.andersson@fmi.fi). CESM source code is distributed through a public subversion code repository (<http://www.cesm.ucar.edu/models/cesm1.0/>). The Atmospheric Chemistry Experiment (ACE), also known as SCISAT, is a Canadian-led mission mainly supported by the Canadian Space Agency and the Natural Sciences and Engineering Research Council of Canada. We are grateful to NASA for providing the MLS Aura data.

References

- Andersson, M. E., P. T. Veronen, C. J. Rodger, M. A. Clilverd, and A. Seppälä (2014), Missing driver in the Sun-Earth connection from energetic electron precipitation impacts mesospheric ozone, *Nat. Commun.*, 5(5197), doi:10.1038/ncomms6197.
- Baumgaertner, A. J. G., A. Seppälä, P. Jöckel, and M. A. Clilverd (2011), Geomagnetic activity related NO_x enhancements and polar surface air temperature variability in a chemistry climate model: Modulation of the NAM index, *Atmos. Chem. Phys.*, 11, 4521–4531, doi:10.5194/acp-11-4521-2011.
- Bernath, P. F., et al. (2005), Atmospheric chemistry experiment (ACE): Mission overview, *Geophys. Res. Lett.*, 3, L15S01, doi:10.1029/2005GL022386.
- Damiani, A., M. Storini, M. Laurenza, and C. Rafanelli (2008), Solar particle effects on minor components of the Polar atmosphere, *Ann. Geophys.*, 26, 361–370, doi:10.5194/angeo-26-361-2008.
- Damiani, A., et al. (2012), Impact of January 2005 solar proton events on chlorine species, *Atmos. Chem. Phys.*, 12, 4159–4179, doi:10.5194/acp-12-4159-2012.
- Froidevaux, L., et al. (2008), Validation of Aura microwave limb sounder HCl measurements, *J. Geophys. Res.*, 113, D15S25, doi:10.1029/2007JD009025.
- Funke, B., et al. (2011), Composition changes after the "Halloween" solar proton event: The High-Energy Particle Precipitation in the Atmosphere (HEPPA) model versus MIPAS data intercomparison study, *Atmos. Chem. Phys.*, 11, 9089–9139, doi:10.5194/acp-11-9089-2011.
- Funke, B., M. López-Puertas, G. P. Stiller, and T. von Clarmann (2014), Mesospheric and stratospheric NO_y produced by energetic particle precipitation during 2002–2012, *J. Geophys. Res.*, 119, 4429–4446, doi:10.1002/2013JD021404.
- Gillet, N. P., and D. W. J. Thompson (2003), Simulation of recent Southern Hemisphere climate change, *Science*, 302, 273–275.
- Jackman, C. H., R. D. McPeters, G. J. Labow, E. L. Fleming, C. J. Praderas, and J. M. Russell (2001), Northern Hemisphere atmospheric effects due to the July 2000 solar proton events, *Geophys. Res. Lett.*, 28, 2883–2886.
- Jackman, C. H., M. T. DeLand, G. J. Labow, E. L. Fleming, D. K. Weisenstein, M. K. W. Ko, M. Sinnhuber, and J. M. Russell (2005), Neutral atmospheric influences of the solar proton events in October–November 2003, *J. Geophys. Res.*, 110, A09S27, doi:10.1029/2004JA010888.
- Jackman, C. H., et al. (2008), Short- and medium-term atmospheric constituent effects of very large solar proton events, *Atmos. Chem. Phys.*, 8, 765–785, doi:10.5194/acp-8-765-2008.
- Jackman, C. H., et al. (2011), Northern Hemisphere atmospheric influence of the solar proton events and ground level enhancement in January 2005, *Atmos. Chem. Phys.*, 11, 6153–6166, doi:10.5194/acp-11-6153-2011.
- Jiang, Y. B., et al. (2007), Validation of Aura Microwave Limb Sounder Ozone by ozonesonde and lidar measurements, *J. Geophys. Res.*, 112, D24S34, doi:10.1029/2007JD008776.
- Kerzenmacher, T., et al. (2008), Validation of NO_2 and NO from the Atmospheric Chemistry Experiment (ACE), *Atmos. Chem. Phys.*, 8, 5801–5841.
- Kvissel, O.-K., Y. J. Orsolini, F. Stordal, I. S. A. Isaksen, and M. L. Santee (2012), Formation of stratospheric nitric acid by a hydrated ion cluster reaction: Implications for the effect of energetic particle precipitation on the middle atmosphere, *J. Geophys. Res.*, 117, D16301, doi:10.1029/2011JD017257.
- Livesey, N. J., et al. (2011), EOS MLS Version 3.3 Level 2 data quality and description document, *Tech. Rep. JPL D-33509*, Jet Propul. Lab., Version 3.3x-1.0, Pasadena, Calif.
- Marsh, D. R., R. R. Garcia, D. E. Kinnison, B. A. Boville, F. Sassi, S. C. Solomon, and K. Matthes (2007), Modeling the whole atmosphere response to solar cycle changes in radiative and geomagnetic forcing, *J. Geophys. Res. Atmos.*, 112, D23306, doi:10.1029/2006JD008306.
- Marsh, D. R., M. Mills, D. Kinnison, J.-F. Lamarque, N. Calvo, and L. Polvani (2013), Climate change from 1850 to 2005 simulated in CESM1(WACCM), *J. Clim.*, 26(19), 7372–7391, doi:10.1175/JCLI-D-12-00558.
- Newham, D. A., P. J. Espy, M. A. Clilverd, C. J. Rodger, A. Seppälä, D. J. Maxfield, P. Hartogh, K. Holmén, and R. B. Horne (2011), Direct observations of nitric oxide produced by energetic electron precipitation into the Antarctic middle atmosphere, *Geophys. Res. Lett.*, 38, L20104, doi:10.1029/2011GL048666.
- Nieder, H., H. Winkler, D. R. Marsh, and M. Sinnhuber (2014), NO_x production due to energetic particle precipitation in the MLT region: Results from ion chemistry model studies, *J. Geophys. Res. Space Physics*, 119, 2137–2148, doi:10.1002/2013JA019044.

- Pickett, H. M., W. G. Read, K. K. Lee, and Y. L. Yung (2006), Observation of night OH in the mesosphere, *Geophys. Res. Lett.*, 33, L19808, doi:10.1029/2006GL026910.
- Pickett, H. M., et al. (2008), Validation of Aura Microwave Limb Sounder OH and HO₂ measurements, *J. Geophys. Res.*, 113, D16S30, doi:10.1029/2007JD008775.
- Porter, H. S., C. H. Jackman, and A. E. S. Green (1976), Efficiencies for production of atomic nitrogen and oxygen by relativistic proton impact in air, *J. Chem. Phys.*, 65, 154–167.
- Randall, C. E., V. L. Harvey, D. E. Siskind, J. France, P. F. Bernath, C. D. Boone, and K. A. Walker (2009), NO_x descent in the Arctic middle atmosphere in early 2009, *Geophys. Res. Lett.*, 36, L18811, doi:10.1029/2009GL039706.
- Reinecker, M. M., et al. (2008), The GEOS-5 data assimilation system: A documentation of GEOS-5.0, *Tech. Rep. 104606 V27*, NASA Goddard Space Flight Center, Greenbelt, Md.
- Rozanov, E., L. Callis, M. Schlesinger, F. Yang, N. Andronova, and V. Zubov (2005), Atmospheric response to NO_y source due to energetic electron precipitation, *Geophys. Res. Lett.*, 32, L14811, doi:10.1029/2005GL023041.
- Rozanov, E., M. Calisto, T. Egorova, T. Peter, and W. Schmutz (2012), The influence of precipitating energetic particles on atmospheric chemistry and climate, *Surv. Geophys.*, 33, 483–501, doi:10.1007/s10712-012-9192-0.
- Salmi, S.-M., P. T. Verronen, L. Thölix, E. Kyrölä, L. Backman, A. Y. Karpeckha, and A. Seppälä (2011), Mesosphere-to-stratosphere descent of odd nitrogen in February–March 2009 after sudden stratospheric warming, *Atmos. Chem. Phys.*, 11, 4645–4655, doi:10.5194/acp-11-4645-2011.
- Santee, M. L., et al. (2007), Validation of the Aura Microwave Limb Sounder HNO₃ measurements, *J. Geophys. Res.*, 112, D24S40, doi:10.1029/2007JD008721.
- Santee, M. L., et al. (2008), Validation of the Aura Microwave Limb Sounder ClO measurements, *J. Geophys. Res.*, 113, D15S22, doi:10.1029/2007JD008762.
- Seppälä, A., P. T. Verronen, V. F. Sofieva, J. Tamminen, E. Kyrölä, C. J. Rodger, and M. A. Clilverd (2006), Destruction of the tertiary ozone maximum during a solar proton event, *Geophys. Res. Lett.*, 33, L07804, doi:10.1029/2005GL025571.
- Seppälä, A., P. T. Verronen, M. A. Clilverd, C. E. Randall, J. Tamminen, V. F. Sofieva, L. Backman, and E. Kyrölä (2007), Arctic and Antarctic polar winter NO_x and energetic particle precipitation in 2002–2006, *Geophys. Res. Lett.*, 34, L12810, doi:10.1029/2007GL029733.
- Seppälä, A., M. A. Clilverd, C. J. Rodger, P. T. Verronen, and E. Turunen (2008), The effects of hard-spectra solar proton events on the middle atmosphere, *J. Geophys. Res.*, 113, A11311, doi:10.1029/2008JA013517.
- Seppälä, A., C. E. Randall, M. A. Clilverd, E. Rozanov, and C. J. Rodger (2009), Geomagnetic activity and polar surface air temperature variability, *J. Geophys. Res.*, 114, A10312, doi:10.1029/2008JA014029.
- Solomon, S., D. W. Rusch, J.-C. Gérard, G. C. Reid, and P. J. Crutzen (1981), The effect of particle precipitation events on the neutral and ion chemistry of the middle atmosphere: II. Odd hydrogen, *Planet. Space Sci.*, 8, 885–893.
- Verronen, P. T., and R. Lehmann (2013), Analysis and parameterisation of ionic reactions affecting middle atmospheric HO_x and NO_y during solar proton events, *Ann. Geophys.*, 31, 909–956, doi:10.5194/angeo-31-909-2013.
- Verronen, P. T., A. Seppälä, E. Kyrölä, J. Tamminen, H. M. Pickett, and E. Turunen (2006), Production of odd hydrogen in the mesosphere during the January 2005 solar proton event, *Geophys. Res. Lett.*, 33, L24811, doi:10.1029/2006GL028115.
- Verronen, P. T., M. L. Santee, G. L. Manney, R. Lehmann, S.-M. Salmi, and A. Seppälä (2011), Nitric acid enhancements in the mesosphere during the January 2005 and December 2006 solar proton events, *J. Geophys. Res.*, 116, D17301, doi:10.1029/2011JD016075.
- Verronen, P. T., M. E. Andersson, D. R. Marsh, T. Kovács, and J. M. C. Plane (2016), WACCM-D—Whole Atmosphere Community Climate Model with D-region ion chemistry, *J. Adv. Model. Earth Syst.*, 8, 954–975, doi:10.1002/2015MS000592.
- Waters, J. W., et al. (2006), The Earth Observing System Microwave Limb Sounder (EOS MLS) on the Aura satellite, *IEEE Trans. Geosci. Remote Sens.*, 44, 1075–1092, doi:10.1109/TGRS.2006.873771.
- Winkler, H., S. Kazeminejad, M. Sinnhuber, M.-B. Kallenrode, and J. Notholt (2009), Conversion of mesospheric HCl into active chlorine during the solar proton event in July 2000 in the northern polar region, *J. Geophys. Res.*, 114, D00103, doi:10.1029/2008JD011587.